

Temperature-dependent pressure broadened line shape measurements in the $\nu_1 + \nu_3$ band of acetylene using a diode laser referenced to a frequency comb

M.J. Cich · C.P. McRaven · G.V. Lopez · T.J. Sears ·
D. Hurtmans · A.W. Mantz

Received: 8 September 2011 / Revised version: 17 October 2011 / Published online: 22 November 2011
© Springer-Verlag 2011

Abstract Using an extended cavity diode laser referenced to a femtosecond frequency comb, the P(11) absorption line in the $\nu_1 + \nu_3$ combination band of the most abundant isotopologue of pure acetylene was studied at temperatures of 296, 240, 200, 175, 165, 160, 155, and 150 K to determine pressure-dependent line shape parameters at these temperatures. The laser emission profile, the instrumental resolution, is a Lorentz function characterized by a half width at half the maximum emission (HWHM) of $8.3 \times 10^{-6} \text{ cm}^{-1}$ (or 250 kHz) for these measurements. Six collision models were tested in fitting the experimental data: Voigt, speed-dependent Voigt, Rautian–Sobel’man, Galatry, and two Rautian–Galatry hybrid models (with and without speed-dependence). Only the speed-dependent Voigt model was able to fit the data to the experimental noise level at all temperatures and for pressures between 3 and nearly 360 torr. The variations of the speed-dependent Voigt profile line shape parameters with temperature were also character-

ized, and this model accurately reproduces the observations over their entire range of temperature and pressure.

1 Introduction

During the last decade the development of phase-locked optical frequency combs in the near infrared has revolutionized metrology and optical clocks [1–4], and the technology has been applied to the measurement of molecular spectra [5–8]. In the near-infrared spectral region, the technology is particularly attractive because of the availability of highly efficient detectors, tunable diode lasers, and Er-doped fiber combs. External cavity diode lasers (ECDLs) also permit continuous coverage of wide spectral regions, frequently providing continuous coverage of entire infrared bands [9]. In a first report of the application of these techniques to precision line shape measurements, we recently described the determination of pressure broadening, narrowing, and shift parameters in acetylene [10] with an improvement in the precision of two orders of magnitude or more over other current measurement techniques.

Aside from its intrinsic interest, the motivation for our work on low temperature acetylene is provided by measurements in the dense atmosphere of Titan, the largest moon of Saturn, and the detection of acetylene around Jupiter’s poles with the NASA Infrared Telescope by the NASA Cassini spacecraft. Titan’s atmosphere is composed mostly of nitrogen (98.4%) [11], methane (1.4%, but 4.9% close to the surface) and other hydrocarbons, including acetylene. The temperature of Titan’s atmosphere is 94 K at the surface [12], where the pressure is approximately 1.45 times that of the Earth’s atmosphere. Trace amounts of acetylene and other gases have also been detected [13, 14] in the atmosphere by mass spectrometers on fly-by missions. While acetylene

M.J. Cich · G.V. Lopez · T.J. Sears (✉)
Department of Chemistry, Stony Brook University, Stony Brook,
NY 11794, USA
e-mail: trevor.sears@stonybrook.edu

C.P. McRaven · T.J. Sears
Chemistry Department, Brookhaven National Lab, Bldg. 555A,
P.O. Box 5000, Upton, NY 11973, USA

D. Hurtmans
Service de Chimie Quantique et de Photophysique (Atomes,
Molécules et Atmosphères), Université Libre de Bruxelles,
50 Av F. D. Roosevelt CPi 160/09, 10050 Bruxelles, Belgium

A.W. Mantz
Department of Physics, Astronomy and Astrophysics,
Connecticut College, 270 Mohegan Avenue, New London,
CT 06320, USA

has not yet been optically studied in Titan's atmosphere, the 1.5 micron region lies in a window between strong water vapor and methane bands and is therefore convenient for both terrestrial and satellite observations. The acetylene $\nu_1 + \nu_3$ combination band is relatively strong, and the availability of highly precise laboratory data could influence future observational programs to look for acetylene on Titan and other planetary bodies.

High precision data for line pressure broadening and shifting for pure acetylene is, as for other molecules, rare, so the results of this study are rather unique: highly precise measurements and a full line shape parameterization for pure acetylene between 150 and 296 K. Line shape parameterization is essential for modeling remote observations of terrestrial or extra-terrestrial atmospheres. In other work to be published [15], we made complementary measurements of nitrogen broadened line shape data for acetylene. Combined with the precise pressure broadened and shifted data reported here, these data significantly improve our knowledge and understanding of the parameters describing the pressure and temperature-dependent behavior of this isolated spectral line.

2 Experimental

The experimental setup was described in detail previously [10]. The spectrometer at Stony Brook University uses a Menlo Systems FC-1500 Optical Frequency Synthesizer based on a mode-locked erbium fiber laser with a broadened output extending from 1050 to 2100 nm. The output of a 1550 nm ECDL (Sacher TEC 520 with Sacher Pilot PC controller) was offset-locked to a single comb line and served as the spectroscopic source. While scanning, the frequency comb's repetition rate was typically changed by one Hz per step, which moves the optical frequency of the phase locked ECDL by 783 kHz in these experiments. Under these conditions, we found (see Sect. 3.1) the laser emission profile to be best described by a Lorentz function characterized by a half width at half the maximum (HWHM) emission of $8.3 \times 10^{-6} \text{ cm}^{-1}$ (250 kHz). This is larger than typical for the comb-stabilized laser, due to the comparatively fast scan speed needed to complete the measurements. At slower scanning rates, we have measured an upper limit to the HWHM of 105(2) kHz [10].

Part of the output from the ECDL was combined with the comb output in the beat detection unit for locking to the comb. Another part of the stabilized output from the ECDL was directed to a wavemeter (Bristol Instruments, model 621), used to provide a convenient estimate of the laser emission frequency. The main beam was directed through an optical isolator and optically chopped at 50 kHz using an electro-optic amplitude modulator (New Focus model 4104

broadband modulator) and polarizing optics. The probe laser beam was then split into two beams, which served as the signal and reference, using a rotatable half-wave plate and cube polarizer. The two beams were separately imaged onto two identical InGaAs-based receivers (New Focus model 2053). The power imaged on the two detectors was matched under conditions of no signal absorption by adjusting the half-wave plate. The signal in the analytical and reference beams was then detected as the phase independent magnitude ($R^2 = X^2 + Y^2$) of the demodulated 50 kHz 1 f signals using two identical two channel digital lock-in amplifiers (SRS model 830), and the ratio of the two lock-in amplifier output signals yielded the transmission line profile directly. Signals from the two lock-in amplifiers were also separately saved for later analysis.

The acetylene absorption took place in a temperature-controlled copper cell [10, 16]. Cells of length 1.085 and 16.551 cm were used to achieve the desired transmittance depending on whether high pressure or low pressure acetylene samples were employed. The temperature sensors were calibrated model 670 Silicon diodes supplied by Lake Shore Cryogenics with a specified temperature accuracy of 0.125 K at 77 K and 0.105 K at 300 K. The sensor temperature was read by a Lake Shore model 331 temperature readout with a precision of 0.0001 K. The output from one of the temperature sensors was also used to continuously monitor the cell temperature during a scan. An MKS model 690A013TRA 0–1000 torr Baratron capacitance manometer gauge head, with certified accuracy of better than 0.04% across the entire range, was used to calibrate the gauge used in early experiments (MKS 310BHS 1000 torr gauge), resulting in an accuracy of 0.14 torr for these measurements. The new gauge was used for the great majority of the current measurements and pressure accuracy is the quoted 0.04%. Pure acetylene gas (>99.6%, MG gases) was used, and the residual acetone was removed by vacuum pumping over a cold trap maintained at -95°C before use in the experiment. Several samples were checked by mass spectrometry to ensure purity. The cell temperature and sample pressure inside the cell were continuously digitally recorded during each scan. Typically both the temperature and pressure are very stable throughout the experiment, with variations less than $\pm 0.005 \text{ K}$, or 0.1% of the pressure, over the period of a scan. Actually pressure and temperature stability variations at the abovementioned levels are maintained for hours inside the copper cell; temperature and pressure are very well known parameters. Even with this control, temperature and pressure readings are the largest source of experimental error in a properly operating frequency comb system.

Table 1 summarizes the entire set of experimental conditions under which spectra were recorded and analyzed. Note that maximum acetylene pressures at gas sample temperatures below 175 K were limited by the vapor pressure of acetylene.

Table 1 Number of acetylene absorption spectra used in the data analysis listed by corresponding experimental conditions

Pressure range (torr)	296 K	240 K	200 K	175 K	165 K	160 K	155 K	150 K
5–20	1	–	2	–	1	2	5	5
20–50	5	3	3	5	2	3	–	–
50–75	7	7	6	7	3	1	–	–
75–150	6	6	7	9	10	–	–	–
150–300	5	11	13	20	–	–	–	–
300–500	8	7	7	–	–	–	–	–

3 Data analysis

3.1 Introduction

Data analysis involves fitting experimental line shapes using calculated spectra that are the result of taking the convolution product of an instrument line shape (or apparatus function) and a theoretical model describing the line shape that is selected to best fit the experimental data. The absorption line shape and the apparatus function may both be adjusted (or fixed to a predetermined value) in a least squares fit procedure to minimize the residuals in the observed minus calculated ($O - C$) synthetic spectrum to determine the appropriate spectroscopic parameters. As described below, the instrument line shape was determined by the analysis of measurements of a low pressure sample where the absorption profile is a known Gaussian.

The absorption line shape is described by

$$T[l, k(\nu, P)] = 100e^{-lk(\nu, P)}, \quad (1)$$

where l is the absorption path length, $k(\nu, P)$ is the absorption coefficient at wavenumber ν and total pressure P , defining the line profile, and $T[l, k(\nu, P)]$ is the percent transmission of the sample at the wavenumber, ν . For very low pressures, a Gaussian profile was used; and for higher pressures, a variety of models were compared.

3.2 Fitting Gaussian profiles (less than 1 torr pressure gas samples)

Absorption by ambient temperature gaseous samples at very low pressures (less than about 0.8 torr) is characterized by a Doppler broadened, or Gaussian, line profile. Modeling a low-pressure absorption line scanned by a narrow laser characterized by a Lorentzian instrument function involves the convolution of these two profiles, i.e., a Voigt profile. We determined this instrument function by recording a low pressure line known to be described by a simple Gaussian function with its own half width at half maximum absorption (HWHM). We found the laser emission $\text{HWHM} = 8.3 \times 10^{-6} \text{ cm}^{-1}$ (250 kHz), and this was fixed in all subsequent measurement analysis in this work.

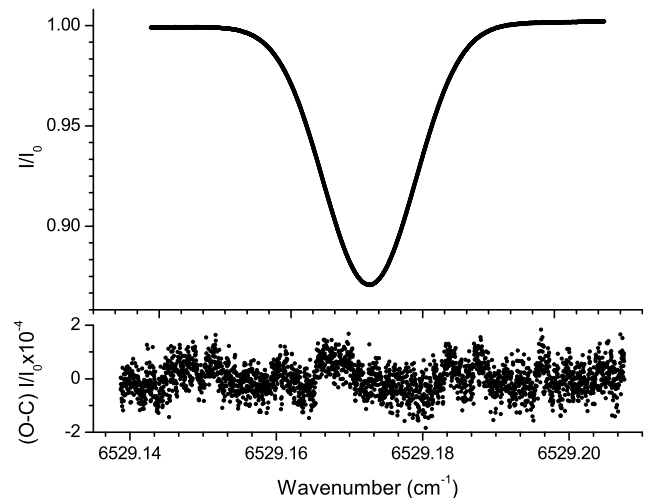


Fig. 1 (Top) Experimental data from a 0.11 torr acetylene sample at 299 K recorded in a cell with an absorption path length of 56.605 cm. (Bottom) Observed minus Calculated residuals ($O - C$) under these conditions resulting from least squares multispectrum fitting of the experimental data to a Gaussian line shape, demonstrating signal-to-noise of approximately 10,000

Figure 1 illustrates the results obtained for a low pressure sample assuming a Gaussian line shape function. The top panel is the spectrum at 299 K. The absorption pathlength is 56.605 cm, and the sample pressure is 0.11 torr. The peak-to-peak residuals shown in the lower panel are approximately 0.0001 of the baseline, or 100% transmission. Although not present in these data, frequently one also encounters a weak fringe in the residuals. These fringes may arise from optical feedback between optical elements, including optical surfaces, spatial filters, etc., and the fringe spacing can change over time due to changes in the room temperature of the laboratory. If there is only one fringe frequency present, it can easily be eliminated from the residuals by including a fringe in the fitting algorithm. Using such fringe reduction techniques, when necessary, we can achieve a fit to the data that has residuals (observed data points minus calculated points from fitting a line shape function, $O - C$) smaller than 0.01% of our I_0 signal.

3.3 Non-Gaussian line profiles (pressure greater than 1 torr)

Higher pressure spectra recorded with the current instrument may also be fit to the level of accuracy mentioned above, and our goal in fitting the spectra is to have residuals that reach the system noise level. Michelson interferometer-controlled tunable diode laser (TDL) measurements routinely achieve fits within the noise level of 0.1% [17]. Data obtained using Fourier transform spectrometers are practically limited to about 0.05% [18] in commercial instruments due to scanning time limitations in achieving satisfactory signal-to-noise ratios (SNR). However, as described below, we find that our residuals at the lowest temperatures and pressures are frequently the result of inadequacies in the line shape models, and not the result of instrument limitations or spectral signal-to-noise.

Absorption by gaseous samples at pressures between approximately 100 and 760 torr can often be characterized by the Voigt or by Lorentzian functions. Both functions provide information about the temperature-dependent collisional lifetime broadening parameter, $\gamma_s(T)$, in case of self-broadening, or $\gamma_f(T)$ in case of broadening by a buffer (or foreign) gas. Pressure shifts in the line center position, δ_s , or δ_f , may also be added to these line shape functions. The pressure shift is generally small and also varies with temperature, but we drop the explicit notation for brevity here and below for all parameters. Absorption profiles characterized by Voigt or Lorentzian functions are always symmetric about the center, unless the absorption feature is a blend of more than one line.

The choice of the proper function to describe absorption lines is not automatic, nor is it generally straightforward. At pressures below about 40 torr, one may encounter narrowing of absorption lines, with the Doppler component of the line narrowing as the total sample pressure increases. This is referred to as Dicke [19, 20], or confinement, narrowing, and characterized by the temperature dependent confinement narrowing parameter, β . As pressure increases, this effect tends to increase, but becomes hidden by the much larger collisional broadening. Dicke narrowing is included in the mathematical formulation of the Galatry soft collision (SOFT) [21], Rautian hard collision (HARD) [22, 23], and the two Rautian/Galatry hybrid models considered below [24, 25].

The HARD model corresponds to the limiting case where the perturbing molecule is much heavier than the absorber, and a significant velocity change of the active molecule requires only one or a few individual collisions. By contrast, the SOFT model corresponds to the case where the perturbing molecule mass is much smaller than the absorber mass, and a significant change in the absorber molecule velocity requires many individual collisions. Large variations in β

may be observed when describing soft or hard collisions at low pressures or when correlations exist between velocity changing and dephasing collisions. Line shifts are also included in these models, but do not significantly depend on the model.

Ciurylo et al. [24] developed a model to describe intermediate cases where a generalized speed-dependent line profile combines soft and hard partially correlated Dicke-narrowing collisions (csdRG). The so-called speed-dependent effects arise because the impact approximation, which assumes that collisions are fast relative to the time between collisions, leads to a Lorentzian line shape, provided collision cross-sections are not a strong function of velocity. However, we know this is not a good assumption as collision cross-sections depend on temperature. This is manifested in the temperature dependence of collision linewidths. Line shapes for each velocity will be Lorentzian, but averaging over relevant velocities yields a line shape function that is a sum of Lorentzians. This results in a Lorentzian line shape near the line center, but in the wings there are significant deviations from Lorentzian line shape in cases where a large number of velocities contribute to the thermal averaging; see Pickett [26] and references therein for more details. The parameter, ε , is introduced in the csdRG model to describe the hardness of the velocity changing collisions, $\varepsilon = 0$ describes a pure soft collision and $\varepsilon = 1$ describes a pure hard collision. Intermediate cases correspond to $0 < \varepsilon < 1$. Hurtmans et al. [27] adopted the use of the so-called “mean persistence velocity ratio”, u_{12} , defined by Chapman and Cowling [28] to take into account the intermediate case perturbing mass ratio. Using Hurtmans et al.’s approach, $\varepsilon_{\text{calc}} = 1 - u_{12}$, with $\varepsilon_{\text{calc}}$ fixed during the fitting process. The mean persistence velocity ratio is the ratio of the mean value of the velocity of the active molecule, mass m_1 , after collision, to its velocity before collision. For hard spheres this ratio is equal to

$$\mu_{12} = \frac{1}{2}M_1 + \frac{1}{2}M_1^2M_2^{-\frac{1}{2}} \ln[(M_2^{\frac{1}{2}} + 1)M_1^{-\frac{1}{2}}] \quad (2)$$

with $M_1 = m_1/(m_1 + m_2)$ and $M_2 = m_2/(m_1 + m_2)$. In the hard collision limit, $\mu_{12} = 0$, and μ_{12} increases to $\mu_{12} = 1$ in the soft collision limit as the ratio m_1/m_2 of the mass of the active molecule to the perturber mass increases from zero to infinity. When both masses are equal, as is the case in this paper, $\mu_{12} = 0.594$.

In the absence of speed-dependent effects, and if correlations can be neglected, the csdRG model reduces to the Rautian–Galatry Profile (RGP) model, for which only three parameters (γ^0 , β^0 , δ^0) are necessary to fully describe the line profile.

Whenever speed-dependent effects on collision broadening are taken into account, either using a weighted sum of Lorentz profile (WSL) [26, 29] or a speed-dependent Voigt profile (SDV) [29, 30], one must choose, or determine, the leading term representing the interaction potential which is

expressed as a simple power q of the intermolecular separation R ($V \propto R^{-q}$), with q an effective parameter characterizing the interaction range. Also, collisional broadening derived from these models represents the thermally averaged value of the broadening as a function of different absorber speeds. Absorber speed-dependence of the pressure shifts is also taken into account using the same interaction potential, as given by Ward et al. [30]. In case both narrowing effects, confinement narrowing and absorber speed-dependence, are considered, a fifth parameter, the narrowing parameter, must be introduced using convolution product models denoted by WSL*SOFT [31, 32] or WSL*HARD [32] where the resulting profile is the result of a convolution product of a WSL profile with a confinement narrowed profile described by the SOFT [21] or the HARD [23] model.

In analyzing the data for this paper, we considered all of the above models describing collisional line shapes. Experimentally, we found line shape asymmetries were apparent, especially at low pressure, but at all temperatures. Line shape models that include correlations between velocity changing and dephasing collisions such as in [33] did *not* describe the observed asymmetries, and we do not include results from these models in this analysis. Instead, we pursued models that include speed-dependent effects to describe the asymmetry because some of these models did result in fit residuals that are essentially at the spectral noise level.

Line shape models that include collisional narrowing, like SOFT, HARD, or RGP, are completely symmetric, and these models fail to reproduce the spectral asymmetry at low pressures. On the other hand, models including speed-dependence as well as collisional narrowing, like the WSL*SOFT or WSL*HARD, or the csdRG model, add

asymmetry to the line shape, but over-emphasize the narrowing compared to our experimental observations.

The results appear to support the recent observations of Wehr et al. [34, 35], who compared high-resolution absorption measurements of Ar perturbed CO lines with theoretical calculations based on solving a transport/relaxation equation for the appropriate off-diagonal matrix element of the density matrix. In their work, speed-dependent collisional broadening and a solid sphere potential were used to determine Dicke narrowing. Their conclusion was that the magnitude of the Dicke narrowing in the CO–Ar system was 70 to 90% less than predicted from the mass diffusion coefficient and present formulations of the SOFT and HARD models.

4 Discussion

4.1 Discussion of line shape fit residuals

At intermediate pressures, between 4 and 50 torr, a weak asymmetry is observed at all sample temperatures. Figure 2 shows a spectrum recorded with a gas temperature of 150 K and at a pressure of 4 torr. The spectrum in Fig. 2 is recorded using the 1.085 cm absorption path length cell. The entire spectral line was collected in one continuous scan at this pressure. The lower panels show the residuals plotted for several line shape models fitted to the data. Each of the lower panels is plotted with the same vertical scale to facilitate analysis by inspection. The sharp artifacts shown in each panel result from electrical noise pickup in the analog-to-digital converter (ADC) for these particular data but they are so rare that they affect the recorded spectrum only cosmetically.

Fig. 2 Transmission spectrum of the acetylene P(11) line at 4 torr and 150 K and in a 1.085 cm absorption path length. (*Bottom panels*) Residuals ($O - C$) under these conditions resulting from least squares multispectrum fitting of experimental data to the corresponding line shape models

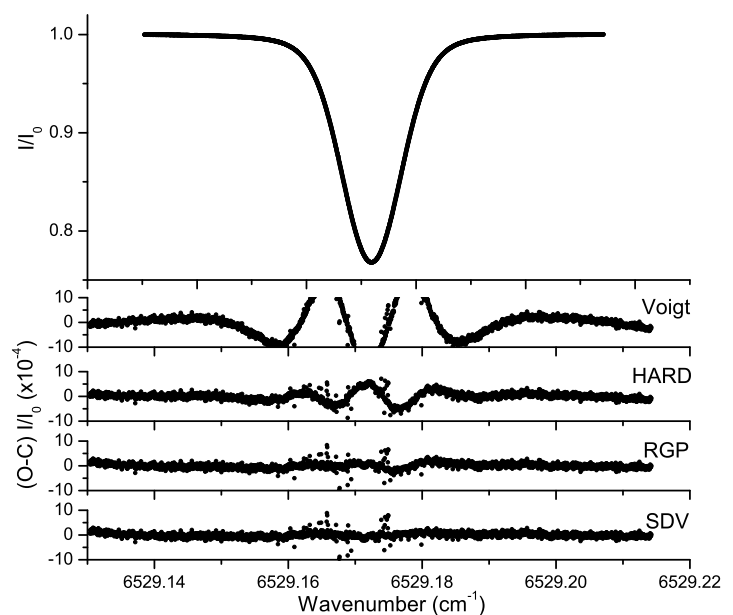
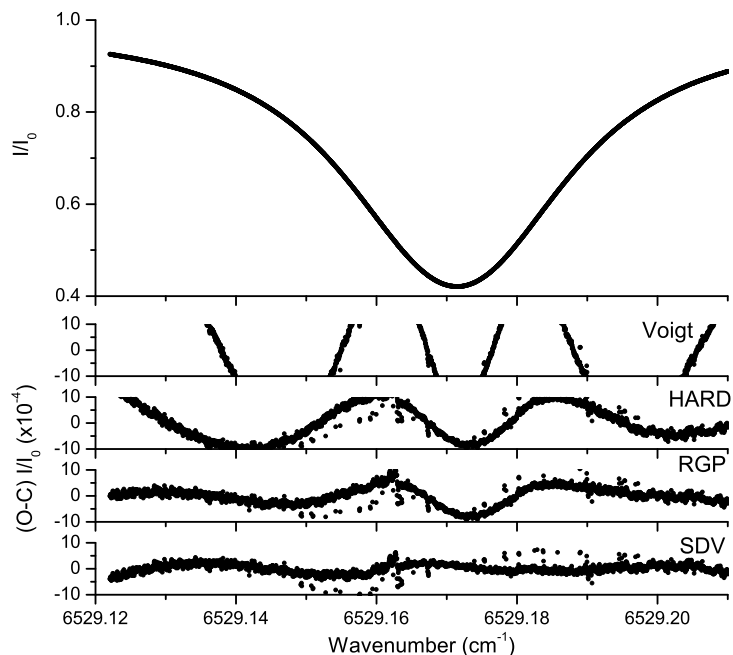


Fig. 3 Transmission spectrum of the acetylene P(11) line at 45 torr and 160 K and a 1.085 cm cell length. (Bottom panels) Residuals ($O - C$) under these conditions resulting from least squares multispectrum fittings of experimental data to the corresponding line shape models



The upper panel in Fig. 2 shows results for a Voigt line shape model. These show the characteristic inverted W shape residuals near the line center commonly associated with this model. In this case, the model is an inappropriate choice due to its oversimplified nature.

The SOFT and HARD models provide residuals that are nearly identical, so we discuss only the HARD ($O - C$) residual results. Clearly, the HARD residuals shown in Fig. 2 are reduced significantly when compared to the Voigt fit. However, the residuals as plotted are still significantly larger than the residual spectral noise level near the line center. It appears that, near line center, collisional narrowing in the HARD model may be too large, as seen in the residuals. However, the fit in the line far wings is quite good.

We found for this study that RGP and csdRG models provided similar residuals when applied to the lowest pressure and lowest temperature spectra. So we discuss only the results from the simpler model, RGP. The RGP residuals in Fig. 2 are significantly closer to the spectral noise level than are the HARD results. In fact, the residuals almost lie at the system spectral noise level, but small asymmetries still exist near line center, and the residuals are approximately two times the size of the spectral noise. The RGP model does not properly model asymmetry, and a small narrowing residual remains.

The fit of the SDV results in the lower panel of Fig. 2 is good to the spectral noise level. Clearly, the SDV model fits the 150 K low pressure spectra best and this was found to be the case for all spectra recorded at 150 K.

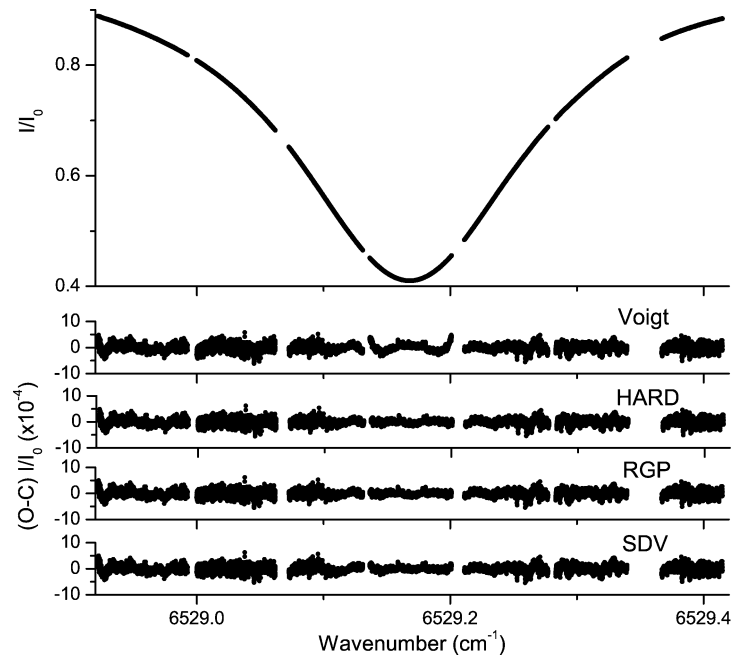
Spectra recorded at higher pressures, where pressure broadening begins to strongly affect the spectral line profile, are generally not as sensitive to the different line profile

functions used to reproduce the experimental spectra. Figure 3 shows a spectrum recorded at 160 K and 45 torr, which is approximately 10 times higher pressure than is plotted in Fig. 2. The entire spectral line was collected in one continuous scan at this pressure.

As before, the residuals associated with each of the four line shape models (convolved with the instrument function) are plotted in the lower panels of Fig. 3. The Voigt profile fit is poor. The HARD residuals are a significant improvement over the Voigt case but remain unsatisfactory. Close inspection shows an asymmetry in the residual, evidence that speed-dependent effects remain. The RGP model residuals are shown below, and are an improvement over the HARD model, but still small asymmetric structure remains. Finally, in the bottom panel, the SDV residuals are within the spectral signal-to-noise ratio. Clearly, the SDV profile provides the best fit at these experimental conditions.

The last spectrum is displayed in Fig. 4. This is a concatenated spectrum in which seven individual experimental files are combined to create one continuous scan over the pressure broadened line. For this spectrum the sample cell and gas were maintained at 200 K at a sample pressure of 352 torr. The gaps in the concatenated scan result from non-overlap of successive scans in this case. However, as we showed before [10] this neither adversely affects the quality of the recorded spectra nor the quality of the spectral analysis. In Figs. 3 and 4, the far wings of these strongly pressure-broadened lines are not shown because they are dominated by the Lorentzian part of the lineshape function that all models reproduce well. Also, although P(11) has no very close absorptions, at the highest pressures and at the lower tem-

Fig. 4 Transmission spectrum of the acetylene line studied here at 352 torr and 200 K and a 1.085 cm cell length. (*Bottom panels*) Residuals ($O - C$) under these conditions resulting from least squares multispectrum fittings of experimental data to the corresponding line shape models



peratures, the effects of the far wings of nearby lines begin to have small effects in its wings.

Analysis of this spectrum results in the panels plotted in the lower part of Fig. 4. The Voigt line shape model fits to the experimental noise level in the wings, but in the region of the line center the residuals take on the characteristic shapes we experienced in Figs. 2 and 3 for this model. Clearly, the Voigt line shape model is inadequate to fit the experimental spectrum to the signal-to-noise level. Yet the great majority of recent publications report results only for analysis of experimental data employing the Voigt line shape model.

All three of the more sophisticated line shape models are adequate to model the spectrum recorded under these conditions, however. The residuals in the same order as for Fig. 3 are shown in the lower panels and fit the data to the experimental signal-to-noise levels. However, the SDV profile is the ONLY profile that fits the data at all temperatures and at all pressures measured, thus we select the SDV profile as the appropriate profile to describe pure acetylene spectra recorded in this study at temperatures between 296 and 150 K, and at pressures between 3 and nearly 360 torr.

These results also emphasize another important fact that cannot be stressed enough: when trying to fit absorption line profiles, one must include low pressure spectra where artifacts may be observed in model fit residuals as well as fits to spectra at a variety of low temperatures. It is inappropriate to claim success with any line shape model unless experimental spectra have been fitted down to pressures of several torr, in addition to including intermediate (several tens of torr) and high pressure spectra (several hundreds of torr). Extrapolation to lower pressures won't work unless one is using

the right model, which is impossible to determine without low pressure measurements.

4.2 Line shape parameter comparison

Considering long term temperature and pressure stability of the sample, accuracy of the wavenumber scale and experimental signal-to-noise ratio, the present line shape data are the most accurate that have been recorded to date for acetylene (and probably any molecule) at near-infrared wavelengths. The experimentally derived pressure parameters are several orders of magnitude more precise than any parameters reported previously for optical work. For these reasons, we report results for the analysis using the four line shape models we considered above, Voigt, HARD, RGP, and SDV, even though the SDV model is clearly the only model that fits all the data to the spectral noise level.

Table 2 summarizes the pressure parameters derived from fitting the experimental data to the Voigt line shape model. The Voigt model includes two pressure dependent parameters, the self-broadening parameter, γ , and the pressure shift parameter, δ . Uncertainties in the fit parameters are expressed in parentheses in units of the last significant figure reported for the parameter, and they are one sigma standard deviation of the least squares fits to the experimental data. Compared to the other models, the errors tend to be higher for the Voigt model. As discussed in Sect. 4.1, the Voigt does not fit to the noise level at any pressure, but at lower pressures it does very poorly. At the severely vapor pressure-limited temperatures of approximately 165 K and below, there is no data taken at high or intermediate pressures and this is a major contribution to the trend of larger

Table 2 Line shape parameters derived from fitting the experimental data to the Voigt line shape model

Average T (K) ^a	Broadening $\gamma(T)$ ^a (cm ⁻¹ /atm)	Shift $\delta(T)$ ^a (cm ⁻¹ /atm)
295.715(19)	0.141755(23)	-0.0076196(132)
240.135(25)	0.144846(71)	-0.0071958(101)
200.298(49)	0.181793(42)	-0.0079120(95)
175.319(16)	0.205407(23)	-0.0077875(281)
165.373(12)	0.214860(46)	-0.0080531(170)
160.343(5)	0.218815(55)	-0.0079847(308)
155.373(3)	0.210408(111)	-0.0074111(349)
150.383(20)	0.207093(144)	-0.0066676(1152)

^aErrors in parentheses are one standard deviation in reference to the last digit shown

Table 3 Line shape parameters derived from fitting the experimental data to the HARD model

Average T (K) ^a	Broadening $\gamma(T)$ ^a (cm ⁻¹ /atm)	Narrowing $\beta(T)$ ^a (cm ⁻¹ /atm)	Shift $\delta(T)$ ^a (cm ⁻¹ /atm)
295.715(19)	0.148057(9)	0.049393(66)	-0.0070613(29)
240.135(25)	0.169874(15)	0.053979(59)	-0.0074234(17)
200.298(49)	0.193347(6)	0.059095(61)	-0.0077966(23)
175.319(16)	0.211161(6)	0.060210(65)	-0.0076641(20)
165.373(12)	0.215287(28)	0.054967(85)	-0.0078360(22)
160.343(5)	0.229150(16)	0.079075(145)	-0.0080484(84)
155.373(3)	0.230106(53)	0.066152(170)	-0.0075890(90)
150.383(20)	0.233411(49)	0.061778(107)	-0.0077810(86)

^aErrors in parentheses are one standard deviation in reference to the last digit shown

uncertainties as temperature decreases. The quoted statistical uncertainties are certainly severe underestimates of the true parameter uncertainties. With reference to Table 2, the pressure broadening parameter shows an increase with lowering temperature until about 165 K. The same may be said of the shift parameter. However, the estimates of both parameters are influenced by the line shape asymmetry resulting from speed-dependent effects, apparent at temperatures below approximately 180 K, and asymmetry is not included in the Voigt model. Figures 2–4 all show the Voigt profile to be inadequate to represent the experimental data, with characteristic inverted W-shaped residuals at all pressures and temperatures.

Table 3 summarizes the pressure parameters obtained from the analysis of the experimental data using the HARD model. The HARD model adds a confinement narrowing, β , to the broadening and shift parameters for a total of three adjustable parameters. The HARD model does not include speed-dependent effects, and as a result, still predicts a sym-

metric line profile. Referring again to Figs. 2 and 3, one can see that the residuals resulting from fitting the experimental data at lower pressures to the HARD model have significant systematic residuals near line center, and the residuals are slightly asymmetric. The highest pressure data, such as that shown in Fig. 4, shows no sign of asymmetry, and is adequately represented by the model. However, since the line shape model must fit all the data at all pressures and at all temperatures, we reject the HARD model since its fit is inadequate at lower temperatures and at the lowest pressures.

Table 4 summarizes the results obtained from the analysis utilizing the RGP model for collisions between identical molecules. As previously mentioned, the RGP model applies when dealing with identical molecules involved in hard or soft collisions. This model incorporates as many as four parameters: the familiar γ , β , and δ , as well as ζ , the first order line mixing coefficient in the Rosenkranz approximation [36]. The asymmetry resulting from ζ is dispersion-like. Additionally, as mentioned earlier, the collision partner mass ratio is accounted for in this model.

Since the values for ζ calculated using this model are rather small, suggesting weak line mixing, except at temperatures below 165 K, we include in Table 4 the results from both sets of calculations, one with $\zeta = 0$, and the other with ζ floating. Except for the data at 240 K, the two sets of constants are similar, but they do differ in value by up to 3 \times or 4 \times the quoted uncertainty (one standard deviation expressed in units of the last significant figure quoted). These models reproduce the experimental data rather well, except at the lowest temperatures and intermediate pressures. Even under the conditions of lowest temperature and pressure, the deviation from noise level is very small, perhaps a factor of two larger than the spectral noise. At higher pressure and temperature, the fits cannot be distinguished from each of the other line shape models, excluding the Voigt.

Table 5 summarizes the results obtained by incorporating the SDV profile to describe the experimental spectra. The SDV model incorporates a pressure broadening, γ , pressure shift, δ , first order line mixing, ζ , and the exponent of the leading term of the power series expansion of the intermolecular potential, q . This is an “effective” potential to the extent it describes the region of the potential explored during the collision trajectory. The SDV model yielded a value for q ranging between 6.2 and 7.5 depending upon the temperature of the colliding gas molecules. Again, values for ζ ranged very close to zero for temperatures above 175 K, so we also constrained ζ to zero, and refit the data, with almost identical results for the pressure parameters. In Tables 4 and 5, the magnitude of ζ increases to lower temperatures. This suggests that line mixing due to overlap of far wings from adjacent lines may become more important at lower temperatures.

Table 4 Line shape parameters derived from fitting the experimental data to the RGP model

Average T (K) ^a	Broadening $\gamma(T)$ ^a (cm ⁻¹ /atm)	Narrowing $\beta(T)$ ^a (cm ⁻¹ /atm)	Shift $\delta(T)$ ^a (cm ⁻¹ /atm)	Mixing (1/atm) ^a
295.715(19)	0.148023(9)	0.060272(60)	-0.0069809(29)	-0.006232(127)
295.715(19)	0.148220(8)	0.060433(62)	-0.0070609(24)	0
240.135(25)	0.168364(23)	0.09646(62)	-0.0073904(20)	0.007194(235)
240.135(25)	0.168476(23)	0.059829(63)	-0.0074118(18)	0
200.298(49)	0.193052(11)	0.071429(64)	-0.0078059(19)	-0.003850(191)
200.298(49)	0.193044(11)	0.071415(64)	-0.0078071(21)	0
175.319(16)	0.211641(7)	0.077032(79)	-0.0076399(26)	-0.002203(257)
175.319(16)	0.208240(27)	0.071018(61)	-0.0074891(27)	0
165.373(12)	0.217151(30)	0.068323(108)	-0.0077639(50)	-0.008762(474)
165.373(12)	0.217076(30)	0.068137(108)	-0.0078455(24)	0
160.343(5)	0.226040(8)	0.080120(83)	-0.0079068(46)	-0.014123(423)
160.343(5)	0.226086(8)	0.080251(85)	-0.0079439(46)	0
155.373(3)	0.233233(52)	0.086025(190)	-0.0077396(193)	-0.01496(198)
155.373(3)	0.233315(51)	0.086224(188)	-0.0076071(81)	0
150.383(20)	0.238734(37)	0.085462(97)	-0.0073896(100)	-0.05705(119)
150.383(20)	0.238243(38)	0.087404(99)	-0.0077763(60)	0

^aErrors in parentheses are one standard deviation in reference to the last digit shown

Table 5 Line shape parameters derived from fitting the experimental data to the SDV model

Average T (K) ^a	Broadening $\gamma(T)$ ^a (cm ⁻¹ /atm)	Shift $\delta(T)$ ^a (cm ⁻¹ /atm) ^a	Mixing (1/atm) ^a	q^a
295.715(19)	0.149912(8)	-0.0076763(21)	0	6.67(1)
295.715(19)	0.149864(9)	-0.0076354(45)	0.001870(185)	6.66(1)
240.135(25)	0.175658(40)	-0.0079908(20)	0	7.42(1)
240.135(25)	0.175718(37)	-0.0080640(52)	0.008462(562)	7.43(1)
200.298(49)	0.197660(16)	-0.0081652(15)	0	6.71(0.6)
200.298(49)	0.197671(60)	-0.0080445(68)	-0.012958(707)	6.71(0.6)
175.319(16)	0.217219(14)	-0.0081368(24)	0	6.840(7)
175.319(16)	0.217117(15)	-0.0082791(57)	0.016713(613)	6.80(1)
165.373(12)	0.226071(8)	-0.0081864(14)	0	6.72(0.5)
165.373(12)	0.227901(31)	-0.0080725(51)	-0.013537(452)	7.23(1)
160.343(5)	0.228853(10)	-0.0081859(31)	0	6.24(0.5)
160.343(5)	0.228870(10)	-0.0082449(100)	0.005501(878)	6.25(0.6)
155.373(3)	0.238473(61)	-0.0079458(73)	0	7.61(3)
155.373(3)	0.238065(60)	-0.0086304(195)	0.072230(1917)	7.51(2)
150.383(20)	0.241989(28)	-0.0081638(40)	0	7.27(0.9)
150.383(20)	0.241926(28)	-0.0078970(98)	-0.032892(1112)	7.25(8)

^aErrors in parentheses are one standard deviation in reference to the last digit shown

4.3 Temperature dependence of the pressure broadening and pressure shift parameters

Since the SDV model is the only model that satisfactorily describes the experimental data to the noise level, we will not pursue a further discussion of the temperature dependence of the pressure broadening or the pressure shift parameters derived from the other models considered above.

Using the notation consistent with the HITRAN database [37], we describe the temperature dependence of the pressure broadening coefficient, γ , as a power law dependence

$$\frac{\gamma(T)}{\gamma_{T_{ref}}} = \left(\frac{T_{ref}}{T}\right)^n, \tag{3}$$

where $\gamma(T)$ is the pressure broadening parameter at temperature T (in Kelvin), T_{ref} is 295.715(19) K, the average for our reference temperature (which wasn't exactly 296 K), and the exponent, n , is the value that minimizes the residuals in the least squares residuals plot of the natural logarithm of these two ratios. Figure 5 is a plot of the natural logarithms of these two ratios for the SDV model results. Statistical errors for both temperature and pressure in this plot are smaller than the points on the graph. The value for n , with its error, derived from this plot is, for $\zeta = 0$,

$$n = 0.7035(61). \tag{4}$$

When the shift values determined when ζ is allowed to float are used instead, $n = 0.7038(66)$ was found. The error obtained from one standard deviation in the plot in Fig. 5 was 0.0050% (3.5×10^{-3}). However, this does not take into account our temperature error, so we approximated the total error by also finding the standard deviation in the related plot

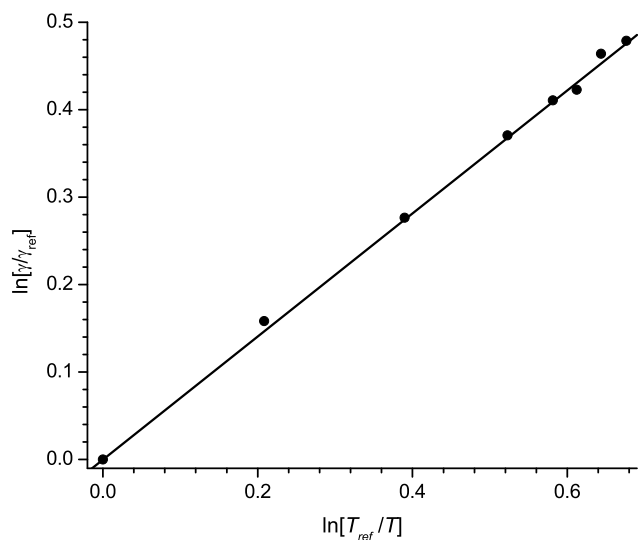


Fig. 5 A plot of the experimentally determined temperature broadening parameters $\gamma(T)$ from Table 5 (SDV model) with line mixing parameter $\zeta = 0$ versus the sample temperature. The slope of this plot determines the temperature dependence exponent n from (3). Error bars for both axes are smaller than the plotted points

for (3) with a slope of $1/n$ (0.0071%) and taking the square root of the sum of the squares of these two standard deviations to get the error shown in (4). The error is expressed in units of the last digit shown for n . The power law dependence shown here is the result of fitting all of the data between 150 and 296 K (shown in Table 5). There is some scatter in the data below 200 K due primarily to the fact that the vapor pressure of acetylene limits the maximum value of the pressure employed experimentally.

The temperature dependence of the pressure shift parameter is best described by the relation recently adopted by Devi et al. [38] as shown in (5) below:

$$\delta(T) = \delta_{T_{ref}} + \delta' \times (T - T_{ref}). \tag{5}$$

Here $\delta(T)$ is the pressure shift coefficient at temperature T (in Kelvin), and δ' describes the temperature dependence of this parameter. This form is employed for the pressure shift coefficient because the sign of the shift can change with change in temperature, unlike the normal behavior of the pressure broadening coefficient. Figure 6 shows the result of plotting a modified form of (5). The experimental data are shown along with their one sigma error bars, and the linear least squares fit to the data is plotted as a straight line. The slope of this plot provides a value for the temperature dependence of the pressure shift parameter. The best least squares fit value for the pressure shift parameter is, for $\zeta = 0$,

$$\delta' = 0.00000400(50) \text{ cm}^{-1}/(\text{atm K}). \tag{6}$$

The error in (6) above is expressed in units of the last digit shown for δ' and is obtained using the same method

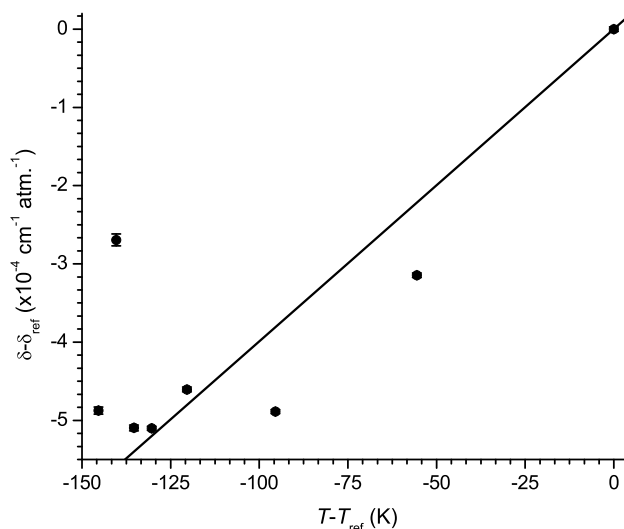


Fig. 6 A plot of the difference between the experimental value of δ at temperature T and the δ at 295.7 K (T_{ref}) to determine the temperature dependence of the pressure shift parameter in the SDV model with $\zeta = 0$ (Table 5). The temperature dependence is designated by the parameter δ' from (5). Error bars for the vertical axis are one standard deviation as listed in Table 5; the error bars are in some cases smaller than the plotted points

as was used in (4). The corresponding value for the case when line mixing (ζ) is included in the model is $4.20(88) \times 10^{-6} \text{ cm}^{-1}/(\text{atm K})$.

The large scatter in the values for δ seen in Fig. 6 is the result of a small line asymmetry in the measured absorption line. This is the reason the speed-dependent Voigt function was the function selected to provide the smallest residuals, at the noise level of the experimental spectra. Even with the excellent fits to the experimental data, the determination of a value for the pressure shift parameter is significantly affected by the resulting line asymmetry. The scatter is also due partially to the fact that speed-dependence also leads to line narrowing, which will significantly affect pressure shift measurements.

5 Conclusions

This is the first detailed study of acetylene in the 1.5 micron region in which line shape models were applied to spectra collected at temperatures ranging from 150 K to room temperature. Our results show that the speed-dependent Voigt profile is the most suitable profile of those tested for describing the absorption line shape for this band of pure acetylene at temperatures between 296 and 150 K. The most commonly used line shape models (i.e., Voigt, Rautian, and Galatry) do not include speed-dependent terms and do very poorly when modeling the line asymmetries we have discovered at lower pressures and especially at low temperatures. The precision of the fitted parameters reported in this paper (and in [10]) is several orders of magnitude better than any values for this band of acetylene published to date as can be seen in Table 5. Using the speed-dependent Voigt data we also derived, for the first time, the power law temperature dependence for the pressure broadening parameter and the temperature dependence for the pressure shift parameter. The precision of these results is due to the extremely accurate frequency scale associated with the optical frequency comb laser employed in this research.

Acknowledgements Acknowledgment is made to the Donors of the American Chemical Society Petroleum Research Fund for partial support of this research. We are grateful for Program Development Funding awarded to TJS by Brookhaven National Laboratory which provided funds for some of the equipment used in this work. CPM gratefully acknowledges support by DOE EPSCoR grant DOE-07ER46361 for work conducted at the University of Oklahoma. AWM gratefully acknowledges support by NASA EPSCoR Grant No. PS 4990 for supporting the development of low temperature cells. The measurements and analyses were performed under grants NNX09AJ93G and NNX08AO78G from the NASA Planetary and Atmospheres program. Work at Brookhaven National Laboratory was carried out under Contract No. DE-AC02-98CH10886 with the US Department of Energy, Office of Science, and supported by its Division of Chemical Sciences, Geosciences and Biosciences within the Office of Basic Energy Sciences.

References

1. Th. Udem, R. Holzwarth, T.W. Hänsch, *Nature* **416**, 233 (2002)
2. D.J. Jones, S.A. Diddams, J.K. Ranka, A. Stenz, R.S. Windeler, J.L. Hall, S.T. Cundiff, *Science* **288**, 635 (2000)
3. S.A. Diddams, D.J. Jones, J. Ye, S.T. Cundiff, J.L. Hall, J.K. Ranka, R.S. Windeler, R. Holzwarth, T. Udem, T.W. Hänsch, *Phys. Rev. Lett.* **84**, 5102 (2000)
4. B.R. Washburn, S.A. Diddams, N.R. Newbury, J. Nicholson, M.F. Yan, C.G. Jurgensen, *Opt. Lett.* **29**, 250 (2004)
5. S.A. Diddams, L. Hollberg, V. Mbele, *Nature* **445**, 627 (2007)
6. I. Coddington, W.C. Swann, N.R. Newbury, *Phys. Rev. Lett.* **100**, 013902(4) (2008)
7. B. Bernhardt, A. Ozawa, P. Jacquet, M. Jacquy, Y. Kobayashi, T. Udem, R. Holzwarth, G. Guelachvili, T.W. Hänsch, N. Picque, *Nat. Photonics* **4**, 55 (2010)
8. Ch. Gohle, B. Stein, A. Schliesser, T. Udem, T.W. Hänsch, *Phys. Rev. Lett.* **99**, 263902 (2007)
9. S.W. Arteaga, C.M. Bejger, J.L. Gerecke, J.L. Hardwick, Z.T. Martin, J. Mayo, E.A. McIlhattan, J.-M.F. Moreau, M.J. Pilkenton, M.J. Polston, B.T. Robertson, E.N. Wolf, *J. Mol. Spectrosc.* **243**, 253 (2007)
10. C.P. McRaven, M.J. Cich, G.V. Lopez, T.J. Sears, D. Hurtmans, A.W. Mantz, *J. Mol. Spectrosc.* **266**, 43 (2011)
11. A. Coustenis, *Space Sci. Rev.* **116**, 171 (2005)
12. C.P. McKay, J.B. Pollack, R. Courtin, *Science* **253**, 1118 (1991)
13. P. Drossart, B. Bezard, S. Atreya, J. Lacy, E. Serabyn, A. Tokunaga, T. Encrenaz, *Icarus* **66**, 610 (1986)
14. H.B. Niemann, S.K. Atreya, S.J. Bauer, G.R. Carignan, J.E. Demick, R.L. Frost, D. Gautier, J.A. Haberman, D.N. Harpold, D.M. Hunten, G. Israel, J.I. Lunine, W.T. Kasprzak, T.C. Owen, M. Paulkovich, F. Raulin, E. Raaen, S.H. Way, *Nature* **438**, 779 (2005)
15. M.J. Cich, C.P. McRaven, G.V. Lopez, T.J. Sears, D. Hurtmans, A.W. Mantz (2011, to be published)
16. A.W. Mantz, V. Malathy-Devi, D.C. Benner, M.A.H. Smith, A. Peredoi-Cross, M. Dulick, *J. Mol. Struct.* **742**, 99 (2005)
17. A. Valentin, A. Henry, C. Claveau, D. Hurtmans, A.W. Mantz, *Mol. Phys.* **102**, 1793 (2004)
18. K. Sung, A.W. Mantz, M.A.H. Smith, L.R. Brown, T.J. Crawford, V. Malathy-Devi, D.C. Benner, *J. Mol. Spectrosc.* **262**, 122 (2010)
19. R.H. Dicke, *Phys. Rev.* **89**, 472 (1953)
20. J.P. Wittke, R.H. Dicke, *Phys. Rev.* **103**, 620 (1956)
21. L. Galatry, *Phys. Rev. Lett.* **122**, 1218 (1961)
22. M. Nelkin, A. Ghatak, *Phys. Rev.* **135**, A4 (1964)
23. S.G. Rautian, I.I. Sobel'man, *Sov. Phys. Usp.* **9**, 701 (1967)
24. R. Ciurylo, A.S. Pine, J. Szudy, *J. Quant. Spectrosc. Radiat. Transf.* **68**, 257 (2001)
25. D. Hurtmans, G. Dufour, W. Bell, A. Henry, A. Valentin, C. Camy-Peyret, *J. Mol. Spectrosc.* **215**, 128 (2002)
26. H.M. Pickett, *J. Chem. Phys.* **73**, 6090 (1980)
27. D. Hurtmans, A. Henry, A. Valentin, C. Boulet, *J. Mol. Spectrosc.* **254**, 126 (2009)
28. S. Chapman, T.G. Cowling, *The Mathematical Theory of Non-uniform Gases* (Cambridge University Press, New York, 1958)
29. P.R. Berman, *J. Quant. Spectrosc. Radiat. Transf.* **12**, 1331 (1972)
30. J. Ward, J. Cooper, E.W. Smith, *J. Quant. Spectrosc. Radiat. Transf.* **14**, 555 (1974)
31. P. Duggan, P.M. Sinclair, A.D. May, J.R. Drummond, *Phys. Rev. A* **51**, 218 (1995)
32. A. Henry, D. Hurtmans, M. Margottin-Maclou, A. Valentin, *J. Quant. Spectrosc. Radiat. Transf.* **56**, 647 (1996)
33. A.S. Pine, *J. Quant. Spectrosc. Radiat. Transf.* **62**, 397 (1999)
34. R. Wehr, R. Ciurylo, A. Vitcu, F. Thibault, J.R. Drummond, A.D. May, *J. Mol. Spectrosc.* **235**, 54 (2006)
35. R. Wehr, A. Vitcu, F. Thibault, J.R. Drummond, A.D. May, *J. Mol. Spectrosc.* **235**, 69 (2006)

36. P.W. Rosenkranz, *IEEE Trans. Antennas Propag.* **AP23**, 498 (1975)
37. L.S. Rothman, I.E. Gordon, A. Barbe, D.C. Benner, P.E. Bernath, M. Birk, V. Boudon, L.R. Brown, A. Campargue, J.P. Champion, K. Chance, L.H. Coudert, V. Dana, V.M. Devi, S. Fally, J.M. Flaud, R.R. Gamache, A. Goldman, D. Jacquemart, I. Kleiner, N. Lacome, W.J. Lafferty, J.Y. Mandin, S.T. Massie, S.N. Mikhailenko, C.E. Miller, N. Moazzen-Ahmadi, O.V. Naumenko, A.V. Nikitin, J. Orphal, V.I. Perevalov, A. Perrin, A. Predoi-Cross, C.P. Rinsland, M. Rotger, M. Simeckova, M.A.H. Smith, K. Sung, S.A. Tashkun, J. Tennyson, R.A. Toth, A.C. Vandaele, J. Vanderauwera, *J. Quant. Spectrosc. Radiat. Transf.* **110**, 533 (2009)
38. V.M. Devi, D.C. Benner, L.R. Brown, C.E. Miller, R.A. Toth, *J. Mol. Spectrosc.* **242**, 90 (2007)